Development of reactive MgO-based Engineered Cementitious Composite (ECC) through accelerated carbonation curing

Hao-liang Wu

Ph.D. Student, Jiangsu Key Laboratory of Urban Underground Engineering & Environmental Safety, Institute of Geotechnical Engineering, Southeast University, Nanjing 210096, China; Joint Ph.D. student at the University of Michigan, US

Email: wuhaoliang90@163.com

Duo Zhang

Postdoctoral Fellow, Department of Civil and Environmental Engineering, University of Michigan, Ann Arbor, MI, 48109, USA

Email: duzhang@umich.edu

Brian R. Ellis

Assistant Professor, Department of Civil and Environmental Engineering, University of Michigan, Ann Arbor, MI, 48109, USA

Email: brellis@umich.edu

Victor C. Li*

Professor, Department of Civil and Environmental Engineering, University of Michigan, Ann Arbor, MI, 48109, USA.

*Corresponding author, Email: vcli@umich.edu

Abstract

The use of reactive magnesium oxide (MgO) is widely recognized in carbonated concrete formulations associated with permanent sequestration of CO_2. Engineered Cementitious Composite (ECC) is an advanced fiber reinforced cement-based composite with high tensile ductility and intrinsically tight crack width. In this paper, we investigate an alternative binary binding system for ECC: reactive MgO and fly ash cured with an accelerated carbonation process. Compressive strength, density, carbonation depth, tensile performance and crack pattern of the carbonated reactive MgO-based ECC were investigated at various curing ages. In addition, the CO_2 uptake and materials sustainability, in terms of energy consumption, net CO_2 emission and cost of the newly developed ECC were assessed. The objective of this research is to further advance the application of reactive MgO and utilization of CO_2 in the construction industry through novel ECC material. It was observed that carbonation curing densifies the binding system, thus leading to an increase in both compressive and first cracking tensile strengths of ECC. The tensile strain capacity of the carbonated reactive MgO-based ECC achieved up to 6% with an average crack width below 60 μm after 1-day carbonation. Compared to conventional ECC (M45) and concrete, the 1-day carbonated reactive MgO-based ECC could reduce the net CO_2 emission by 65% and 45%, respectively. It is concluded that environmental and technical benefits could be simultaneously achieved for the 1-day carbonated reactive MgO-based ECC incorporated with 50% fly ash. The findings of this research shed light on further applications of reactive MgO cement in the precast industry.

Keywords: Engineered Cementitious Composite (ECC); reactive MgO; tensile ductility; carbonation curing, CO_2 utilization

1. Introduction

As the cement and concrete industries are facing an increasing pressure of CO_2 emission reduction, intensive efforts have been devoted to developing low-carbon alternative binders [1, 2] and manufacturing approaches [3, 4]. Among emerging alternative binders, reactive MgO has demonstrated an outstanding ability to sequester CO_2 as compared to Portland cement (PC) [5, 6]. A relatively lower temperature is needed for the calcination process of the reactive MgO (i.e., 700 - 1000°C for reactive MgO vs. 1450°C for PC), thus allowing the use of alternative fuels with relativity low heating values (e.g., refuse-derived fuel and hybrid) [7]. The reactive MgO forms the binding property through reacting with H_2O and CO_2 to sequester CO_2 and gain strength [8-12]. **Eq. 1** shows the hydration of MgO while **Eqs. 2 - 4** represent the carbonation reactions. The hydration product of MgO, i.e., brucite, contributes little to no bonding capability, hence demanding a sufficient carbonation degree to form desirable strengths. To do so requires an intentional carbonation process to allow transformation of MgO to a variety of hydrated magnesium carbonates, mainly including nesquehonite, hydromagnesites and dypingite. The ability of fixing gaseous CO_2 through MgO carbonation has spurred interest in utilizing CO_2 to develop carbonated reactive MgO as a binder for building materials.

$$MgO + H_2O \rightarrow Mg(OH)_2 \text{ (brucite)} \quad (1)$$

$$Mg(OH)_2 + CO_2 + 2H_2O \rightarrow MgCO_3 \cdot 3H_2O \text{ (nesquehonite)} \quad (2)$$

$$5Mg(OH)_2 + 4CO_2 \rightarrow 4MgCO_3 \cdot Mg(OH)_2 \cdot 4H_2O \text{ (hydromagnesites)} \quad (3)$$

$$5Mg(OH)_2 + 4CO_2 + H_2O \rightarrow 4MgCO_3 \cdot Mg(OH)_2 \cdot 5H_2O \text{ (dypingite)} \quad (4)$$

The use of carbonated reactive MgO as a binder faces two intrinsic barriers: (1) the strength development largely relies on carbonation, thus a porous microstructure with small thickness is preferred in facilitating CO_2 diffusion; and (2) reduction in pH of pore solution increases the risk of steel depassivation, hence limiting the application of steel reinforcements [6, 9]. These two barriers restrict the application of the carbonated reactive MgO to producing non-structural porous materials at small scale, which are of limited usage in the precast industry.

The needs of further exploring applications of reactive MgO binder with high CO_2 sequestration capacity and production efficiency motivated this study. Engineered Cementitious Composite (ECC) could be a promising candidate for this purpose [13]. ECC represents a class of high tensile ductility materials with strain-hardening and multiple-cracking behavior [14, 15]. The tensile strain capacity of ECC is normally over 3%, nearly 300 times that of conventional concrete [16]. The high tensile ductility could reduce the necessities of incorporating steel reinforcements in certain applications, offering opportunities for low-pH binders such as the carbonated reactive MgO [14, 15]. Another unique feature of ECC is that the width of the multiple cracks can be controlled to below 60 μm [17], contributing to a low permeability and enhanced durability in the cracked condition. This tight crack width control is autogenous, without dependence on steel reinforcement. A number of structural applications have highlighted substantial technical benefits of using ECC, e.g., impact resistance, structural rehabilitation and seepage proofing [15, 18].

ECC can be tailored in terms of chemical formulations and micromechanics to accommodate different types of raw ingredients [15]. In conventional ECC, PC and fly ash are the main binding ingredients while synthetic fibers such as PVA, PP and PE fibers serve as reinforcing elements. Driven by interest in developing more sustainable materials, prior investigations have examined a number of mineral admixtures and alternative binders, e.g., ground granulated blast-furnace slag (GGBFS), alkali-activated binders, to develop low-carbon ECC [19-21]. More recently, the carbonated reactive MgO-based binder was introduced to ECC, achieving a tensile strain capacity of up to ~4.0% and an ultimate tensile strength of ~4.1 MPa after 28-day carbonation [13]. Despite the desirable mechanical performance, the carbonation duration was long (7 - 28 days) which lessened application appeals in the precast industry, for which efficient manufacturing is economically critical. Additionally, the environmental and economic impacts associated with the carbonated reactive MgO-based ECC remain uncertain.

In further pushing the application of reactive MgO and improving the production efficiency, an accelerated carbonation curing process that was previously adopted in conventional precast concretes [3, 9, 22-23] is developed here for a reactive MgO-based ECC. The carbonation duration can be shortened to 1 day at an elevated CO_2 pressure. Effects of the accelerated carbonation curing on mechanical properties, cracking behavior and microstructure of the reactive MgO-based ECC are examined.

Sustainability and cost of this new version of ECC are also investigated.

2. Experimental program

2.1. Materials and mix proportion

Light-burnt MgO (MAGOX® premium grade, Premier Magnesia, LLC) and fly ash (class F, Headwaters Resources Inc) were used as binders. 99.5% of the MgO can pass the standard #325 mesh and 100% MgO can pass the #100 mesh, as per ASTM E11 [24]. **Table 1** lists the chemical compositions of the MgO and fly ash. Polyvinyl alcohol (PVA) fibers with 1.2% oil content supplied by Kuraray Ltd. (Japan) were used for the ECC. Mechanical properties of the PVA fiber are listed in **Table 2**. Tap water was used for mixing. To achieve a sufficient workability of the fresh mixture, sodium hexametaphosphate (SHMP, chemical formula: $Na(PO_3)_6$, Alfa Aesar™) [25] and superplasticizer (SP, W.R. Grace & Co.) were applied.

Table 1. Chemical compositions of MgO and fly ash determined by XRF

Chemical component[a]	MgO (%)	FA (%)
SiO_2	0.31	52.19
Al_2O_3	0.2	22.23
SO_3	-	2.16
MgO	95.76	0.93
P_2O_5	-	0.11
K_2O	-	2.56
TiO_2	0.01	1.01
Fe_2O_3	0.13	13.49
CaO	0.81	3.40
Cl	0.03	0.01
Loss on ignition (at 950 ℃)	2.75	1.01

Note: [a] Chemical component is analyzed by X-ray fluorescence method using ARL9800XP+XRF spectrometry

Table 2. Properties of PVA fiber

Length (mm)	Diameter (μm)	Elongation (%)	Density (kg/m^3)	Young's modulus (GPa)	Tensile strength (MPa)
8	39	6	1300	42.8	1600

Two mix proportions were studied with 70% and 50% MgO by the binder's mass, respectively. **Table 3** shows the details of the mix proportions. The two mixtures were denoted as C# and N#, where # referred to MgO content by binder mass (i.e., 0.7 or 0.5). The C# referred to the mixtures subjected to the accelerated carbonation curing, and the N# referred to the non-carbonated reference that was cured in air (T = 20 ± 2□, Relative humidity (RH) = 65 ± 2%).

Table 3. Mix proportions of reactive MgO-based ECC (mass ratio)

Batch ID	MgO	Fly ash	Water	SHMP[a]	SP	PVA Fiber[b]
C0.7, N0.7	0.7	0.3	0.60	0.060	0.0073	2.0
C0.5, N0.5	0.5	0.5	0.52	0.052	0.0073	2.0

[a]SHMP was 10% by water mass;
[b]PVA fiber content was by volume (%)

2.2. Sample preparation

Both mixtures were prepared using a 4-liter mortar mixer. The solid ingredients, including reactive MgO and fly ash, were dry-mixed at 100 rpm for 2 min. A SHMP-SP solution was prepared using the mixing water. SHMP was first added into the mixing water and was stirred for 5 min using a magnetic stirrer at a rate of 240 rad/min and a temperature of 85□. After mixing, SP was added to the solution and was stirred for another 1 min. The SHMP-SP solution was added to the dry ingredients in the mortar mixer and was mixed at 150 rpm for 3 min to produce a uniform matrix. The PVA fibers were then added and were mixed at the same rate for an additional 5 min. The fresh mixtures were cast into cubes (50 mm×50 mm×50 mm) and dogbone-shaped molds (**Fig. 1**) followed by 3-min vibration. These specimens were covered with a plastic sheet to prevent moisture loss and set in air (temperature = 20 ± 2℃ and RH = 65 ± 2%), and were demolded at 21 h after casting.

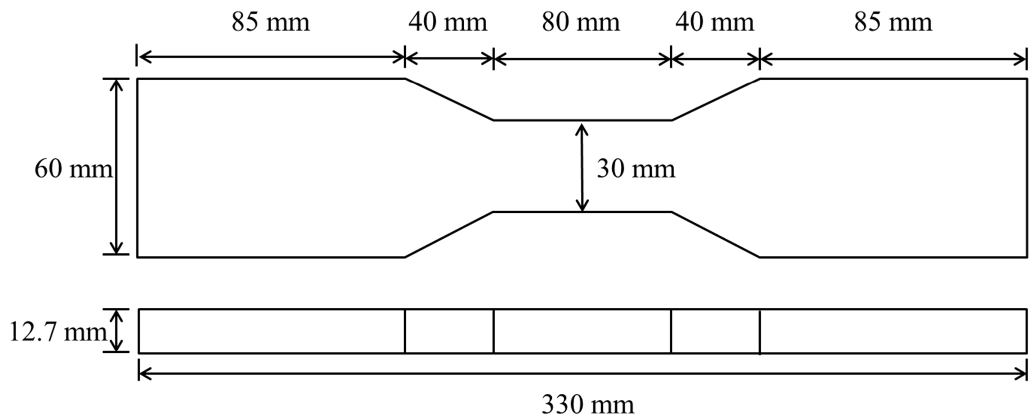

Fig. 1. Dimensions of dogbone-shaped specimen for uniaxial tension test

The reactive MgO-based ECC specimens after demolding were split into two groups, i.e., carbonation-cured ECC (C#) and non-carbonated ECC (N#). To facilitate CO_2 diffusion in ECC, the demolded specimens were placed on a grid plate for a 3-hour de-mold conditioning at temperature of 20 ± 2℃ and RH of 65 ± 2%. The purpose of the de-mold conditioning was to remove excess moisture in the porous space of ECC to provide interconnected pathways for CO_2 diffusion. The reactive MgO-based ECC carbonation was performed in a pressure chamber depicted in **Fig. 2**. The carbonation chamber was continuously supplied with CO_2 gas of 99.8% purity and 2.0 bar pressure (2×10^5 Pa). A tray of water (~100 g) was placed inside the chamber to prevent sample water evaporation during the carbonation process. The cube and dogbone-shaped ECC specimens were carbonated for 1 day, 3 days and 7 days. The specimens' mass changes induced by carbonation curing were recorded.

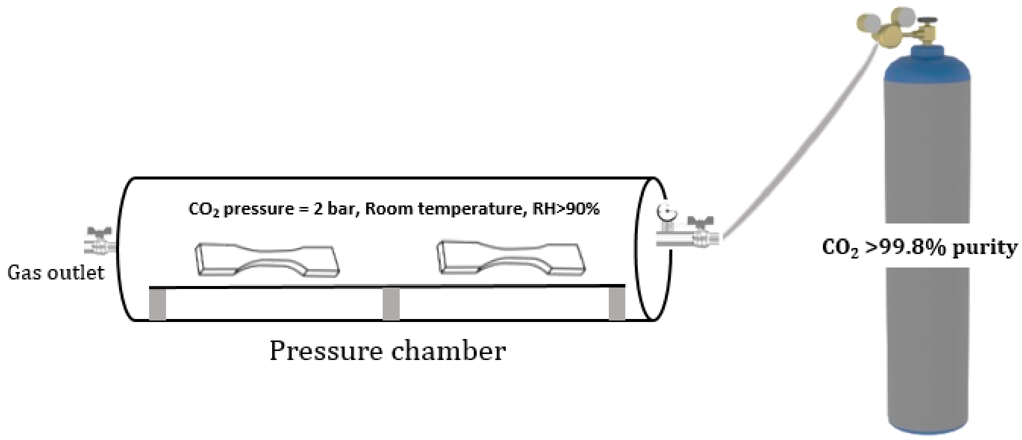

Fig. 2. Laboratory setup for ECC carbonation curing

2.3. Performance evaluation

The compression test was performed on the cube specimens following ASTM C109/C109M [26]. The loading rate was set at 0.34 ± 0.07 MPa/s. Triplicate specimens for each batch were prepared and tested. Phenolphthalein indicator was used to determine the depth of carbonation on the cross section of cubes.

Uniaxial tension test was performed on the dogbone-shaped specimens following the Japan Society of Civil Engineers (JSCE) high performance fiber reinforced cementitious composite testing method [27]. Linear variable displacement transducer (LVDT) was used to measure the tensile deformation. The tension test was conducted using an Instron® instrument (ElectroPlus^{TM} E10000 Linear-Torsion Model) with a loading capacity of 10 kN. The dogbone-shaped specimens were gripped using wedge action on their slanting edges. Sufficient degree of freedom was allowed in the grips to ensure the application of uniaxial tension along the longitudinal axis. The loading rate was 0.5 mm/min. Triplicate specimens were tested for each batch.

Residual crack numbers and widths were measured on the dogbone-shaped specimens in unloaded state after the uniaxial tension using an infinity X-C21 optical electron microscope with a resolution of 10 μm (Hirbor CX-50470RZ, Japan), and the collected images were analyzed using the discriminant analysis method following Li [15]. Triplicate specimens were examined for each observation, and the coefficient of variation (COV) of crack widths and numbers were both found to be less than 5% indicating a good consistency of the measurement.

After tension test, fracture surfaces of the specimens were examined using a JEOL IT500 Scanning Electron Microscope (SEM) at 5 kV accelerating voltage. X-ray diffraction (XRD) was performed using powder samples obtained from the same specimens to estimate CO_2 uptake. The specimens were saw cut to pieces smaller than 10 mm and were manually ground to pass a 30-μm sieve. The powder samples were thoroughly mixed with 10% lithium fluoride (LiF) as an internal reference for conducting quantitative XRD. A Rigaku SmartLab XRD with CuKα radiation was used for the data collection. The X-rays were generated at 40mA and 45kV. A beam knife was used to mitigate air scattering during the scanning. The diffraction pattern was collected in the range of 5° - 70° 2θ with a step size of 0.02° 2θ. Phase quantification was carried out using MDI Jade 2010. The phase contents were regulated to the sample's ignited mass at 1100°C.

3. Results and discussion

3.1. Compressive strength and carbonation depth

Fig. 3 (a) shows the age-dependent evolution of compressive strength for the four different batches of reactive MgO-based ECC. For the non-carbonated reference, the 7-day compressive strength reached 15.92 MPa and 14.23 MPa for the mixes with 70% and 50% reactive MgO (N0.7 and N0.5), respectively. The strength gain in the absence of carbonation was likely attributed to formation of brucite through MgO hydration, as shown in **Eq. 1**. Nevertheless, the contribution of brucite to compressive strength was relatively trivial as compared to that due to carbonation curing. In the carbonation-cured specimens with 70% reactive MgO (C0.7), the compressive strength achieved 22.55 MPa at 1 day. Extending the carbonation duration to 7 days improved the compressive strength to 41.99 MPa (a 86.2% increase). The same trend was observed for the mix with 50% reactive MgO (C0.5), where the compressive strength was improved by 72.5% from 1 day to 7 days and achieved 31.52 MPa after 7-day carbonation. The increase in compressive strength of reactive MgO-based materials enabled by carbonation has been widely recognized in previous studies and is attributed to the precipitation of hydrated magnesium carbonates [5] following **Eqs. 2 - 4**.

Fig 3 (**b**) shows the measured density of the same cube specimens. The trend in evolution of sample density agrees closely with that of compressive strength, i.e., a longer carbonation duration led to a denser binding matrix along with a higher compressive strength. As the carbonation duration increased from 1 day to 7 days, the densities were increased by 23.3% and 14.1% for C0.7 and C0.5, respectively. **Fig. 4** shows the carbonation depth in the same period as determined by phenolphthalein indicator on the cross-section. A nearly twofold increase in carbonation depth was observed between 1-day and 7-day of CO_2 exposure. At 7 days, the cube specimens likely achieved a complete carbonation along the thickness (50 mm) for both mixes as indicated by the carbonation depth (23.7 mm for C0.7 and 25 mm for C0.5).

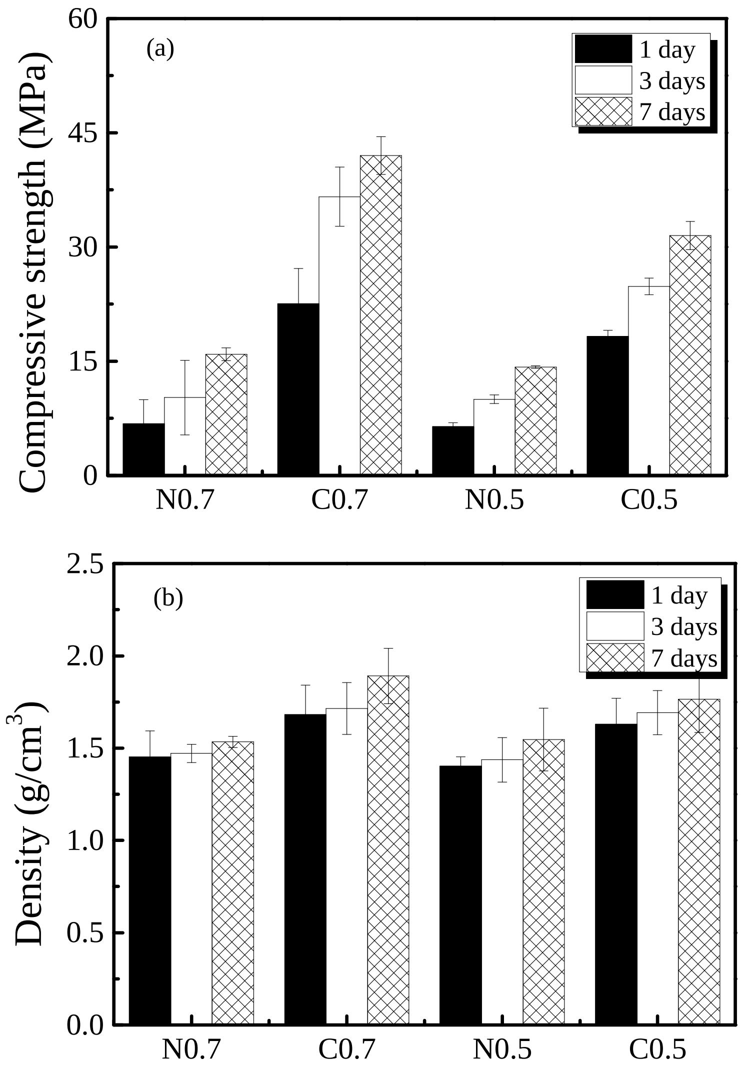

Fig. 3. (a) Compressive strength and (b) density of reactive MgO-based ECC cube specimens

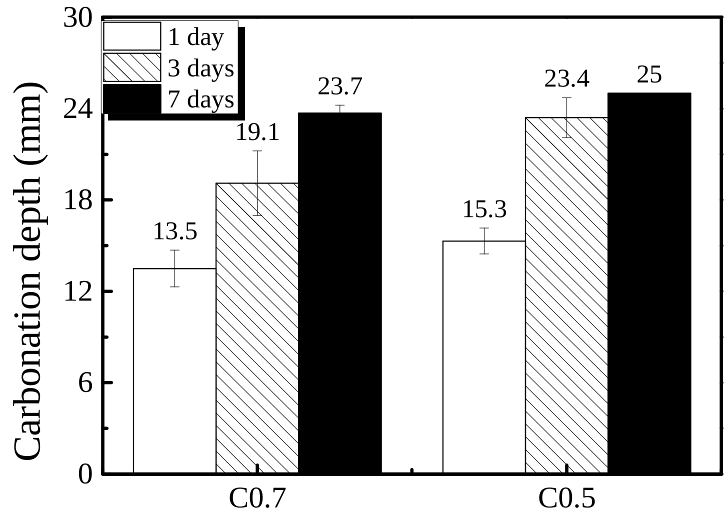

Fig 4. Carbonation depth of reactive MgO-based ECC cube specimens

3.2. Tensile performance

Results of the uniaxial tension tests are shown in the form of stress-strain curves in **Fig. 5**. The tensile stresses recorded at occurrence of the first crack and approaching specimen failure were named as "first cracking strength" and "ultimate tensile strength", respectively. The maximum tensile strain obtained during the tension test was referred to as the specimen's "tensile strain capacity". **Table 4** lists such defined parameters for evaluation of the tensile performance.

As shown in **Fig. 5**, typical elastic and strain-hardening stages were clearly identified for all batches. For the non-carbonated reference made with 70% MgO and 30% fly ash (N0.7), the first cracking strength and tensile strain capacity at 1 day achieved 0.71 MPa and 4.02%, respectively. Introducing carbonation curing doubled the first cracking strength and improved the tensile strain capacity up to 6.04% at 1 day. As indicated by phenolphthalein test on the cross-section, the dogbone-shaped specimen was likely carbonated throughout the thickness at 1 day. Extending the carbonation duration to 7 days led to a further increase in the first cracking strength to 2.85 MPa but substantially decreased the tensile strain capacity to only 3.27%. As compared to reference [13] at 7 days curing, the first cracking strength is almost identical but the tensile strain capacity is higher (5.89% v.s. 2.70%). It was indicated that an optimal condition was reached by carbonation at 1 day, beyond which longer carbonation would result in an excessively strong matrix and consequently reduce the ductility.

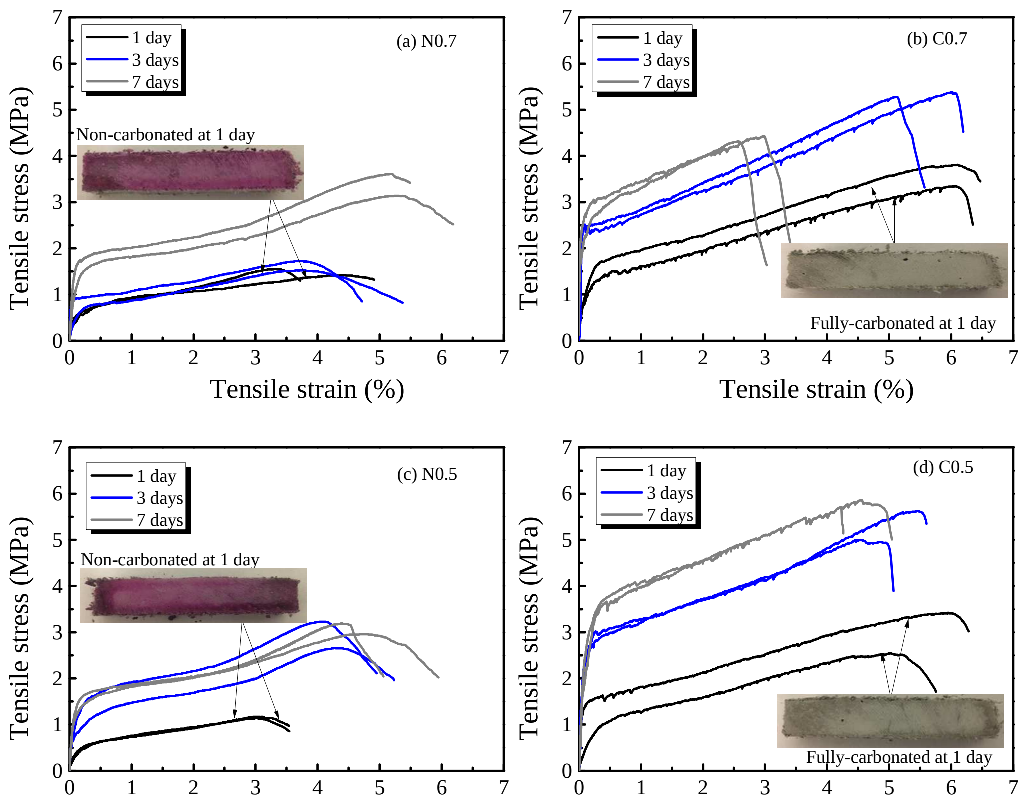

Fig. 5. Uniaxial tensile stress-strain curves for (a) N0.7, (b) C0.7, (c) N0.5, and (d) C0.5 (the inserts show carbonation depth determined by phenolphthalein spray on cross section. Dogbone-shaped specimens were fully-carbonated along the thickness after 1-day carbonation.)

For the non-carbonated reference (N0.7), however, the matrix strength was relatively low at 1 day. With a longer curing time, hydration of the reactive MgO gradually strengthened the matrix through precipitating brucite in the microstructure [13, 28], thus increasing the first cracking strength to 1.72 MPa. The tensile strain capacity of N0.7 increased accordingly with the hydration age. Nevertheless, both the first cracking strength and tensile strain capacity measured in the non-carbonated reference (N0.7) at 7 days appeared lower than those in the carbonation-cured specimen at 1 day (C0.7). These results support that the carbonation curing process developed in this study was an effective approach for achieving desirable mechanical performance of the MgO-based ECC in a timely manner.

Table 4. Uniaxial tensile properties of reactive MgO-based ECC

Batch ID	Curing time (days)	First cracking strength (MPa)	Ultimate tensile strength (MPa)	Tensile strain capacity (%)
N0.7	1	0.71	1.43	4.02
	3	0.87	1.64	3.93
	7	1.72	2.82	5.14
C0.7	1	1.56	3.52	6.04
	3	2.52	5.37	5.79
	7	2.85	4.23	3.27
N0.5	1	0.62	1.19	3.08
	3	0.80	2.68	3.88
	7	1.53	2.89	4.53
C0.5	1	1.73	3.41	5.89
	3	2.75	4.92	4.88
	7	3.62	5.60	4.52

For the carbonation-cured mix with lower MgO content (C0.5 with 50% MgO by weight), the same trend was observed in that the first cracking strength and tensile strain capacity peaked at 1 day and progressively decreased with longer carbonation duration. The highest tensile strain capacity was 5.89% (C0.5 at 1 day) and decreased to 4.52% (C0.5 at 7 days).

3.3. Tensile crack patterns and fracture surface observation

Tensile crack patterns were obtained by counting crack number and measuring crack width along the middle line drawn on the dogbone-shaped specimen in the longitudinal direction as shown in **Fig. 6**. Multiple cracking during the strain-hardening stage largely accommodates the imposed deformation [29]. **Table 5** lists the residual average and total crack widths after peak load at various curing ages. The term "residual crack pattern" was used to indicate that the crack patterns were obtained after releasing the uniaxial tensile load.

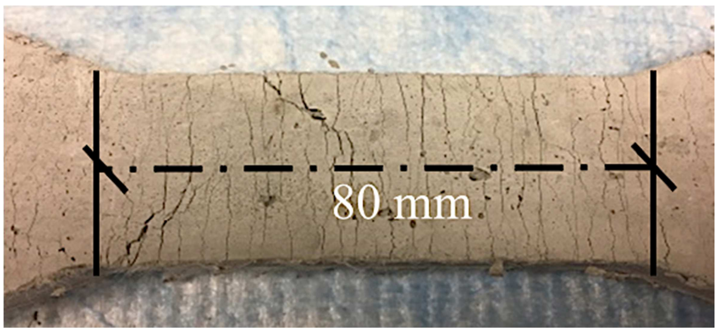

Fig. 6. Typical crack pattern of C0.7 specimen after 1-day carbonation

Table 5. Residual crack widths and numbers obtained on dogbone-shaped specimens

Batch ID	Curing age (days)	Avg. crack width (μm)	Crack number
N0.7	1	33.44	47
	3	30.99	49
	7	21.25	54
C0.7	1	51.95	56
	3	36.05	62
	7	24.18	69
N0.5	1	28.71	43
	3	24.82	44
	7	20.22	47
C0.5	1	30.17	55
	3	25.78	57
	7	22.22	62

Compared to the non-carbonated reference (N0.7 and N0.5), carbonation curing (C0.7 and C0.5) increased the average crack widths and crack numbers at all ages. Extending the carbonation duration tended to increase crack numbers while reducing average crack widths. After 7-day carbonation, the average crack widths decreased to below 25 μm for both C0.7 and C0.5.

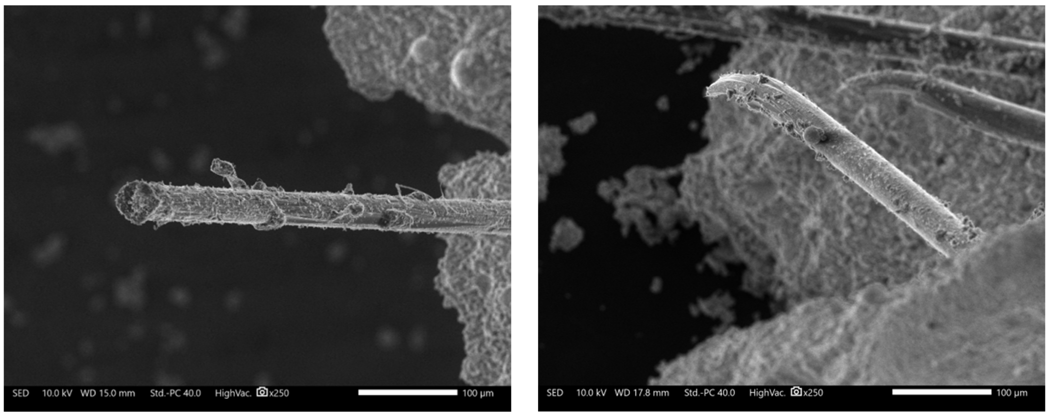

(a) N0.7 (b) C0.7

Fig. 7. SEM images for (a) N0.7 and (b) C0.7 after 7-day curing

SEM images were taken on the fracture surface of C0.7 and N0.7 at 7 days as presented in **Fig. 7**. The purpose of performing SEM observation was to identify the failure mechanism of fiber-matrix bridging, i.e., fiber rupture or fiber pullout. **Fig. 7 (a)** represents a typical fiber pullout observed in the non-carbonated specimens. In comparison, fibers in carbonation-cured specimen displayed a shorter protruded length as shown in **Fig. 7 (b)**. The fiber also seemed to be sharpened at the tip, suggesting fiber rupture following a short pullout stage. In contrast, the non-carbonated reference showed a relatively undamaged fiber tip, suggesting complete fiber pullout without rupture. These observations suggested that a stronger fiber-matrix interfacial bond in the more extensively carbonated specimens (7 days) contributed to fiber rupture that impaired the ECC's strain-hardening capability [30].

3.4. Estimated CO_2 uptake

Table 6 shows the residual MgO and $Mg(OH)_2$ contents determined by XRD (shown in **Fig. 8**) and the associated estimates of CO_2 uptake. All values were regulated to the sample's ignited mass at 1100 °C. In order to estimate the CO_2 uptake, the MgO content in reactive MgO-based ECC was determined by subtracting residual MgO and $Mg(OH)_2$ from the total MgO based on the mix proportion shown in **Table 3**. The amount of CO_2 was obtained by assuming a mole ratio of CO_2 to MgO of 0.8, which represents the lower limit of CO_2 binding capacity in the reactive MgO-based ECC listed in **Eqs. 2 - 4**. As shown in **Table 6**, the CO_2 uptake achieved 34% for C0.7 and 17% for C0.5 after 1-day carbonation. Extending the carbonation duration led to a noticeable increase in the CO_2 uptake and a decrease in the residual amount of MgO and $Mg(OH)_2$.

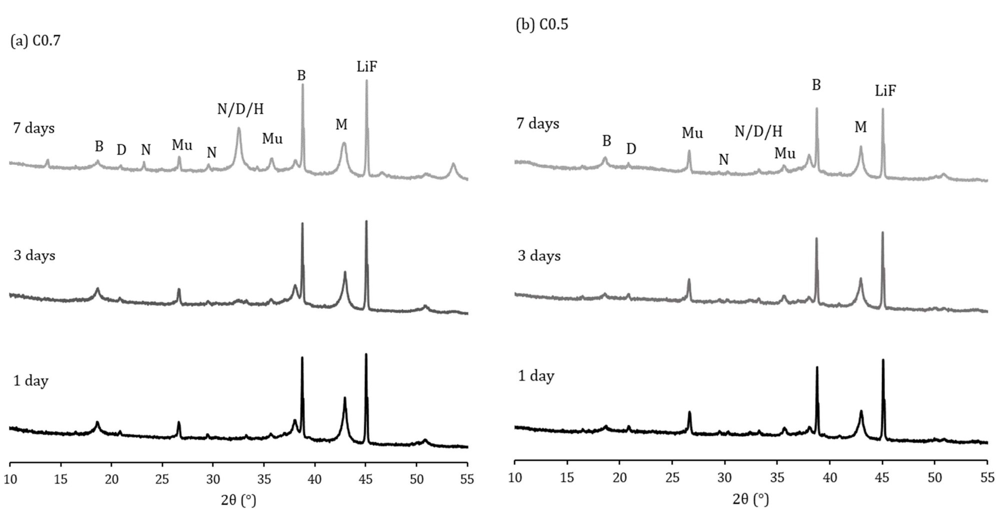

Fig. 8. XRD patterns of (a) C0.7 and (b) C0.5
(B: brucite, D: dypingite, N: nesquehonite, Mu: mullite, H: hydromagnesite, M: MgO, LiF: lithium fluoride (internal reference)

Table 6. Residual contents of MgO, $Mg(OH)_2$ and estimated CO_2 uptake in reactive MgO-based ECC after carbonation curing

Batch ID	Carbonation time (days)	MgO (%)	$Mg(OH)_2$ (%)	Estimated CO_2 uptake by MgO+FA mass (%)	Estimated CO_2 uptake by MgO mass (%)
C0.7	1	12	11	34	49
	3	9	11	35	50
	7	4	7	46	66
C0.5	1	11	16	17	34
	3	9	5	26	52
	7	9	5	26	52

Note: Phase content and CO_2 uptake were based on sample's mass ignited at 1100°C. In Rietveld refinement, Rwp was in range of 4.06-5.41. GOF was in range of 1.73-2.62.

As can be seen in a plot of CO_2 uptake versus carbonation duration shown in **Fig. 9,** the rate of CO_2 uptake in the first three days of carbonation was faster in C0.5 than in C0.7. This is indicative that a higher amount of fly ash may accelerate the process of MgO carbonation. Similar results enabled by adding fly ash have been previously reported in PC systems and were attributed to greater dispersion of reactive particles in the matrix due to incorporation of higher volumes of fly ash [23, 31]. After 7-day carbonation, the CO_2 uptake achieved 46% and 26% by binder's mass in C0.7 and C0.5, respectively. The higher CO_2 uptake attained in C0.7 was expected given the relatively higher portion of reactive MgO in the mix.

The evolution of CO_2 uptake was correlated with the tensile strain capacity as displayed in **Fig. 9**. For the C0.7 mix, the CO_2 uptake slightly varied from 33% (1 day) to 35% (3 days) at a rate of 1.0%/day, but noticeably increased up to 46% after 7 days of carbonation at a rate of 2.7%/day. The decrease in tensile strain capacity showed a corresponding trend, where the rate of change was small from 1 day to 3 days (i.e., from 6.04% to 5.79% in **Table 4**) at a rate of -0.1%/day, but became pronounced when carbonation reached 7 days (3.27%) at a rate of -0.6%/day. The same relationship between tensile strain capacity and CO_2 uptake was confirmed for C0.5.

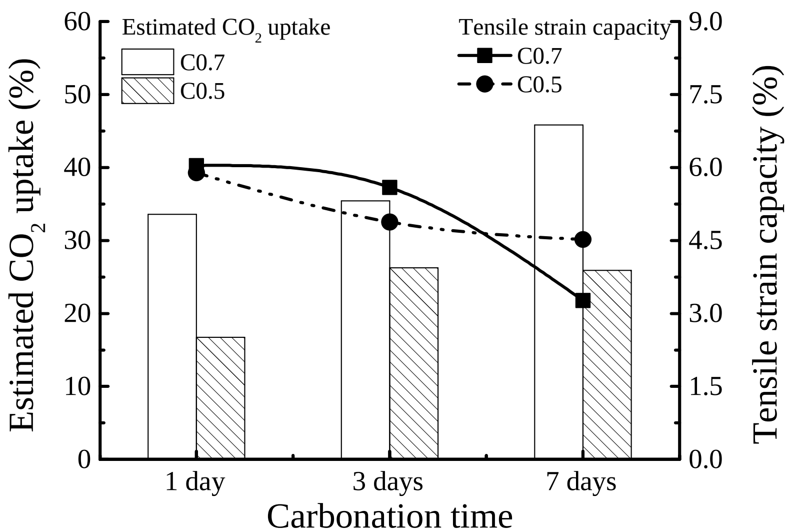

Fig. 9. Relation between estimated CO_2 uptake and tensile strain capacity

The observed decrease of tensile strain capacity with increased carbonation time may be explained through changes in the interfacial bond between the reactive MgO-fly ash matrix and PVA fibers. Greater CO_2 uptake tended to strengthen the matrix and likely led to a stronger fiber-matrix bond allowing less slippage at the interface. Such an increase in the fiber-matrix bond led the fiber to rupture prior to complete pulling out, resulting in loss of tensile ductility. For the mixtures used in this study, it is concluded that 1-day carbonation may be sufficient to achieve desirable tensile ductility while still possessing a prominent capacity for CO_2 sequestration.

3.5. Environmental and economic impacts

Material sustainability indicators (MSIs) were adopted to evaluate the overall environmental and economic factors affecting the sustainability of the reactive MgO-based ECC developed in this study. The MSIs are a set of indictors calculated based on energy and material flow in the manufacturing process [16, 29]. The major MSIs of the reactive MgO-based ECC were chosen as energy consumption, CO_2 emission and material cost, which were collected for each component as shown in **Table 7**. It should be noted that the fly ash was assumed as a waste stream with zero embodied energy consumption and CO_2 emission in this study.

Table 7. Breakdown of embodied energy consumption, CO_2 emission and material cost for ingredients in reactive MgO-based ECC

Component	Energy consumption (GJ/t)	CO_2 emission (kg/t)	Cost (USD/t)
Cement	4.5-6.6[a]	870-940[a,b]	48[e]
MgO	2.4[c]	1400[c]	200[e]
Water	1.2	0.2	7.0[e]
Fly ash	0[a]	0[b]	25.6[e]
Superplasticizer	35[a]	1667[a,b]	1211[e]
$Na(PO_3)_6$	12.8[d]	1065[d]	688[e]
PVA Fiber	101[a]	1710[b]	12670[e]

[a] Data from Pacheco-Torgal et al., (2017) [32].
[b] Data from Keoleian et al., (2005) [33].
[c] Data from Unluer and Al-Tabbaa (2014) [6].
[d] Data from Tripathi (2007) [34].
[e] Market price that may fluctuate.

The MSIs of the reactive MgO-based ECC were calculated on a volume basis and were compared with that of concrete and the conventional version of ECC (M45)

[11] in **Table 8**. The total energy consumption and cost of MgO-based ECC were calculated following **Eq. 5**, where M_{total} denotes total energy/cost of ECC, M_i and F_i denote energy/cost and fraction of mixing component *i*, respectively. The net CO_2 emission of MgO-based ECC was calculated as **Eq. 6**, where C_{total} denotes net CO_2 emission of ECC, C_i and FC_i denote CO_2 emission and fraction of mixing component *i*, respectively. C_0 denotes CO_2 uptake in ECC (**Table 6**).

$$M_{total} = \sum M_i \times F_i \tag{5}$$

$$C_{total} = \sum (C_i \times FC_i) - C_0 \tag{6}$$

Table 8. Comparison of MSIs and cost for concrete, conventional ECC and reactive MgO-based ECC

Material	Energy consumption (GJ/m^3)	Net CO_2 emission (kg/m^3)	Cost (USD/ m^3)
Concrete	2.5 [a]	373 [a]	108 [b]
ECC-M45 [c]	6.7	581	443
ECC-C0.7	3.7	451 - 551	308
ECC-C0.5	1.9	132 - 205	178

[a] Data from Yang et al. (2007) [29].
[b] Data from Portland Cement Association.
[c] Data from Yu and Leung (2017) [35].

The energy consumption, CO_2 emission and cost of conventional ECC (M45) were 2.8, 1.6 and 4.1 times that of concrete, respectively. The high volumes of cement and silica sand, as well as the use of PVA fibers, accounts for these differences. Substituting the Portland cement binding system in ECC-M45 by the reactive MgO-fly ash binder significantly improves the sustainability performance. Compared to ECC-M45, the ECC-C0.7 and ECC-C0.5 have reductions of 44% and 71% in total energy consumption, and of 31% and 60% in production cost, respectively. With

1-day carbonation, the net CO_2 emission of ECC-C0.5 is projected to decrease by up to ~65% compared to that of ECC-M45. It is interesting that the carbonated ECC-C0.5 has an even lower net CO_2 emission compared to the conventional concrete. Despite a higher embodied CO_2 for MgO than Portland cement, net CO_2 emission of ECC-C0.5 is found lower compared to that of conventional concrete due to CO_2 sequestration enabled by carbonation curing. With a tensile strain capacity of 5.89% after 1-day carbonation (**Table 4**), the ECC-C0.5 presents an excellent environmental benefit while possessing a desirable technical performance. Further investigations on durability of this new version of ECC would be helpful in determining life-cycle impacts of its applications in specific structures.

4. Conclusions

A new version of precast ECC was developed based on reactive MgO-fly ash binding system and accelerated carbonation curing process using high purity CO_2 at an elevated pressure of 2 bars. Conclusions can be drawn as follows:

1) Accelerated carbonation curing densified the microstructure of the reactive MgO-based ECC through precipitation of hydrated magnesium carbonates, thus leading to higher compressive strength compared to non-carbonated reference at the same age. First crack strength obtained from uniaxial tension test also increased with increasing duration of carbonation curing.

2) Strain hardening and multiple cracking were clearly identified in the carbonated reactive MgO-based ECC subjected to uniaxial tension. 1-day carbonation led to an increase of the tensile strain capacity from 3.08 - 4.02% (non-carbonated

reference) to 5.89 - 6.04%. However, carbonation curing with durations longer than 1 day progressively reduced the tensile ductility with the lowest observed strain capacities (3.27 - 4.52%) occurring after 7 days of carbonation curing.

3) When the carbonation period increased from 1 to 7 days, the estimated CO_2 uptake, as measured by binder mass, increased from 34% to 46% for mixtures with 70% MgO and from 17% to 26% for those with 50% MgO. The decreasing trend of tensile strain capacity with longer carbonation duration was closely correlated with the trend of CO_2 uptake, indicating that a higher carbonation degree beyond the 1-day carbonation curing was responsible for the reduced tensile ductility for this new version of ECC.

4) With a longer carbonation curing, the average crack width was reduced and the total number of cracks was increased. Compared to the non-carbonated reference, carbonation curing likely created a stronger fiber-matrix interfacial bond and consequently led to increased occurrence of fiber rupture.

5) Compared to the benchmark ECC-M45, the 1-day carbonated reactive MgO-fly ash binding system (with 50% MgO) has lower embodied energy and CO_2, as well as lower cost. The total energy consumption is reduced by ~71%, the net CO_2 emission is reduced by ~65%, and the production cost is reduced by ~60%. With up to 50% fly ash incorporated in the binding system, the new 1-day carbonated ECC version could achieve both technical and environmental benefits for precast applications, with MSIs dropping below those of normal concrete. The findings of this research could be applicated into wall precast concrete pipes and wall panels.

Acknowledgments

The first author is supported by a grant from the Chinese Scholarship Council as a visiting scholar at the University of Michigan. Financial support for this research is partially obtained from the Colleges and Universities in Jiangsu Province Plans to Graduate Research and Innovation (KYLX16_0242), and the Scientific Research Foundation of Graduate School of Southeast University (Grant No. YBJJ1735). Additional financial support by the US Department of Energy (Grant No. DE-FE0030684) is greatly appreciated.

References

[1] Juenger, M., F. Winnefeld, J.L. Provis, and J. Ideker, *Advances in alternative cementitious binders.* Cement and concrete research, 2011. **41**(12): p. 1232-1243.

[2] Shi, C., A.F. Jiménez, and A. Palomo, *New cements for the 21st century: the pursuit of an alternative to Portland cement.* Cement and concrete research, 2011. **41**(7): p. 750-763.

[3] Zhang, D., Z. Ghouleh, and Y. Shao, *Review on carbonation curing of cement-based materials.* Journal of CO2 Utilization, 2017. **21**: p. 119-131.

[4] Ishak, S.A. and H. Hashim, *Low carbon measures for cement plant–a review.* Journal of Cleaner Production, 2015. **103**: p. 260-274.

[5] Unluer, C. and A. Al-Tabbaa, *Impact of hydrated magnesium carbonate additives on the carbonation of reactive MgO cements.* Cement and Concrete Research, 2013. **54**: p. 87-97.

[6] Unluer, C. and A. Al-Tabbaa, *Enhancing the carbonation of MgO cement porous blocks through improved curing conditions.* Cement and Concrete Research, 2014. **59**: p. 55-65.

[7] Shand, M.A., *The chemistry and technology of magnesia*. 2006: John Wiley & Sons.

[8] Dong, H., C. Unluer, E.-H. Yang, and A. Al-Tabbaa, *Recovery of reactive MgO from reject brine via the addition of NaOH.* Desalination, 2018. **429**: p. 88-95.

[9] Vandeperre, L. and A. Al-Tabbaa, *Accelerated carbonation of reactive MgO cements.* Advances in Cement Research, 2007. **19**(2): p. 67-79.

[10] Vandeperre, L., M. Liska, and A. Al-Tabbaa, *Microstructures of reactive magnesia cement blends.* Cement and Concrete Composites, 2008. **30**(8): p. 706-714.

[11] Mo, L., F. Zhang, and M. Deng, *Effects of carbonation treatment on the properties of hydrated fly ash-MgO-Portland cement blends.* Construction and Building Materials, 2015. **96**: p. 147-154.

[12] Abdalqader, A.F., F. Jin, and A. Al-Tabbaa, *Characterisation of reactive magnesia and sodium carbonate-activated fly ash/slag paste blends.* Construction and Building Materials, 2015. **93**: p. 506-513.

[13] Ruan, S., J. Qiu, E.-H. Yang, and C. Unluer, *Fiber-reinforced reactive magnesia-based tensile strain-hardening composites.* Cement and Concrete Composites, 2018. **89**: p. 52-61.

[14] Li, V.C., *On engineered cementitious composites (ECC).* Journal of advanced concrete technology, 2003. **1**(3): p. 215-230.

[15] Li, V.C., *Engineered cementitious composites (ECC) material, structural, and durability performance*. Concrete Construction Engineering Handbook, ed. N. E. 2008: CRC Press.

[16] Li, V.C., M.D. Lepech, S. Wang, M. Weimann, and G. Keoleian, *Development of green ECC for sustainable infrastructure systems.* 2004.

[17] Lepech, M.D. and V.C. Li, *Water permeability of engineered cementitious composites.* Cement and Concrete Composites, 2009. **31**(10): p. 744-753.

[18] Liu, H., Q. Zhang, C. Gu, H. Su, and V.C. Li, *Influence of micro-cracking on the permeability of engineered cementitious composites.* Cement and Concrete Composites, 2016. **72**: p. 104-113.

[19] Qian, S., J. Zhou, M. De Rooij, E. Schlangen, G. Ye, and K. Van Breugel, *Self-healing behavior of strain hardening cementitious composites incorporating local waste materials.* Cement and Concrete Composites, 2009. **31**(9): p. 613-621.

[20] Zhou, J., S. Qian, M.G.S. Beltran, G. Ye, K. van Breugel, and V.C. Li, *Development of engineered cementitious composites with limestone powder and blast furnace slag.*

Materials and Structures, 2010. **43**(6): p. 803-814.
[21] Ohno, M. and V.C. Li, *A feasibility study of strain hardening fiber reinforced fly ash-based geopolymer composites.* Construction and Building Materials, 2014. **57**: p. 163-168.
[22] Zhang, D. and Y. Shao, *Effect of early carbonation curing on chloride penetration and weathering carbonation in concrete.* Construction and Building Materials, 2016. **123**: p. 516-526.
[23] Zhang, D., X. Cai, and Y. Shao, *Carbonation curing of precast fly ash concrete.* Journal of Materials in Civil Engineering, 2016. **28**(11): p. 04016127.
[24] Standard, A., *ASTM-E11 Standard Specification for Woven Wire Test Sieve Cloth and Test Sieves".* 2013.
[25] Zhang, T., C. Cheeseman, and L. Vandeperre, *Development of low pH cement systems forming magnesium silicate hydrate (MSH).* Cement and Concrete Research, 2011. **41**(4): p. 439-442.
[26] ASTM, *C109/C109M "Standard Test Method for Compressive Strength of Hydraulic Cement Mortars (Using 2-in. or [50-mm] Cube Specimens)," ASTM International, West Conshohocken, PA.* 2013.
[27] JSCE, *Recommendations for Design and Construction of High Performance Fiber Reinforced Cement Composites with Multiple Fine Cracks (HPFRCC).* 2008: Tokyo.
[28] Unluer, C. and A. Al-Tabbaa, *The role of brucite, ground granulated blastfurnace slag, and magnesium silicates in the carbonation and performance of MgO cements.* Construction and Building Materials, 2015. **94**: p. 629-643.
[29] Yang, E.-H., Y. Yang, and V.C. Li, *Use of high volumes of fly ash to improve ECC mechanical properties and material greenness.* ACI materials journal, 2007. **104**(6): p. 620.
[30] Şahmaran, M. and V.C. Li, *Durability properties of micro-cracked ECC containing high volumes fly ash.* Cement and Concrete Research, 2009. **39**(11): p. 1033-1043.
[31] Papadakis, V.G., *Effect of supplementary cementing materials on concrete resistance against carbonation and chloride ingress.* Cement and concrete research, 2000. **30**(2): p. 291-299.
[32] Pacheco-Torgal, F., Z. Abdollahnejad, S. Miraldo, and M. Kheradmand, *Alkali-activated cement-based binders (AACBs) as durable and cost-competitive low-CO2 binder materials: some shortcomings that need to be addressed (pp. 195-216).* 2017: Butterworth-Heinemann, Oxford, UK.
[33] Keoleian, G.A., A. Kendall, J.E. Dettling, V.M. Smith, R.F. Chandler, M.D. Lepech, and V.C. Li, *Life cycle modeling of concrete bridge design: Comparison of engineered cementitious composite link slabs and conventional steel expansion joints.* Journal of infrastructure systems, 2005. **11**(1): p. 51-60.
[34] Tripathi, M., *Life Cycle Energy and Emissions for Municipal Water and Wastewater Services: Case-Studies of Treatment plants in the US.* 2007.
[35] Yu, J. and C.K. Leung, *Strength improvement of strain-hardening cementitious composites with ultrahigh-volume fly ash.* Journal of Materials in Civil Engineering, 2017. **29**(9): p. 05017003.